ACS APPLIED MATERIALS & INTERFACES

Research Article

Cite This: ACS Appl. Mater. Interfaces 2017, 9, 39576-39583

www.acsami.org

All-in-One Graphene Based Composite Fiber: Toward Wearable Supercapacitor

Lucas Lim,[†,‡] Yangshuai Liu,[†,‡] Wenwen Liu,[†] Ricky Tjandra,[†] Lathankan Rasenthiram,[†] Zhongwei Chen,[†] and Aiping Yu*[,†]

[†]Department of Chemical Engineering, Waterloo Institute for Nanotechnology, University of Waterloo, Waterloo, Ontario N2L 3G1, Canada

Supporting Information

ABSTRACT: Graphene fibers (GF) have aroused great interest in wearable electronics applications because of their excellent mechanical flexibility and superior electrical conductivity. Herein, an all-in-one graphene and MnO_2 composite hybrid supercapacitor fiber device has been developed. The unique coaxial design of this device facilitates large-scale production while avoiding the risk of short circuiting. The core backbone of the device consists of GF that not only provides mechanical stability but also ensures fast electron transfer during charge−discharge. The introduction of a MnO_2 (200 nm in length) hierarchical nanostructured film enhanced the pseudocapacitance dramatically compared to the graphene-only device in part because of the abundant number of active sites in contact with the poly(vinyl alcohol) (PVA)/H_3PO_4 electrolyte. The entire device exhibits outstanding mechanical strength as well as good electrocapacitive performance with a volumetric capacitance of 29.6 F cm^{-3} at 2 mv s^{-1}. The capacitance of the device did not fade under bending from 0° to 150°, while the capacitance retention of 93% was observed after 1000 cycles. These unique features make this device a promising candidate for applications in wearable fabric supercapacitors.

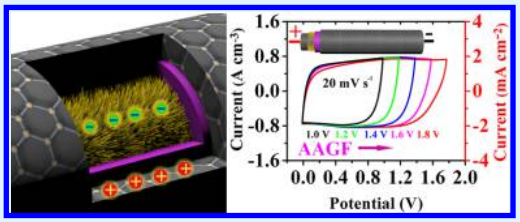

KEYWORDS: *graphene fiber, hybrid supercapacitor, manganese dioxide, flexible supercapacitor, wearable electronics*

INTRODUCTION

Portable and wearable electronic devices have continuously attracted attention and represent a mainstream direction in modern electronics.[1,2] Fabrication of highly flexible fibrous materials has been extensively pursued to meet these specific demands. For instance, the remarkable flexibility of polymer fibers makes them well suited as a possible material for structural support and scaffolding. However, their poor electrical conductivity greatly limits their potential as electrode materials.[3,4]

The discovery of liquid crystal graphene oxide paves the path for designing graphene-based microscopic structures including graphene foams, sponges, and fibers.[5−7] Among these structures, graphene fibers (GFs)/yarns have arisen as widely used materials in both academia and industry owing to their extraordinary properties in mechanical flexibility and electrical conductivity.[8−10] GF has significant value as it opens up possibilities for integration with other materials and functional groups for increased performance and properties. Recently, some efforts have been made to apply GFs to wearable electronic devices.[11−18] Usually, GF is constructed by a tremendous number of 2-D graphene sheets. However, the utilization of 2-D graphene sheets still presents difficulties in creation of GF with high mechanical strength or notable performance. The primary challenges involve difficulties in fabrication of continuous and highly ordered graphene sheets with strong interactions between the sheets layers. For GF to function in energy-storage applications such as supercapacitors, an additional obstacle is the difficulty of simultaneously achieving mechanical flexibility, high performance, and scalability. Most current GF supercapacitors suffer from low capacitance and low mechanical strength because of the absence of pseudocapacitance or poor design.[15,19] The lack of an effective, low-cost, and convenient assembly strategy has hindered further development of GF supercapacitors.

In this regard, recent studies tried to address the already mentioned problems. For instance, GF supercapacitor devices have been designed by using laser reduction of GO fibers.[20,21] However, the high cost, ultralow capacitance, and inherently weak backbone GO fiber of these GF supercapacitors make them less attractive for practical applications. It has been proven by many studies that the introduction of a transitional metal oxide such as MnO_2 should tremendously increase the capacitance of neat graphene.[6,22−26] However, the combination of homogeneous and ultrafine MnO_2 with GF is a challenge in itself. $KMnO_4$ is usually used to directly oxidize graphene sheets and to form MnO_2 coatings on their surface, but this process may dramatically change the nature of the fiber because of strong oxidation. Moreover, the size of formed MnO_2 particles is usually uncontrollable, and the particles are naturally agglomerated. Thus, generation of MnO_2 in moderated condition is strongly required.

Received: July 26, 2017
Accepted: October 25, 2017
Published: November 3, 2017

DOI: 10.1021/acsami.7b10182
ACS Appl. Mater. Interfaces 2017, 9, 39576−39583

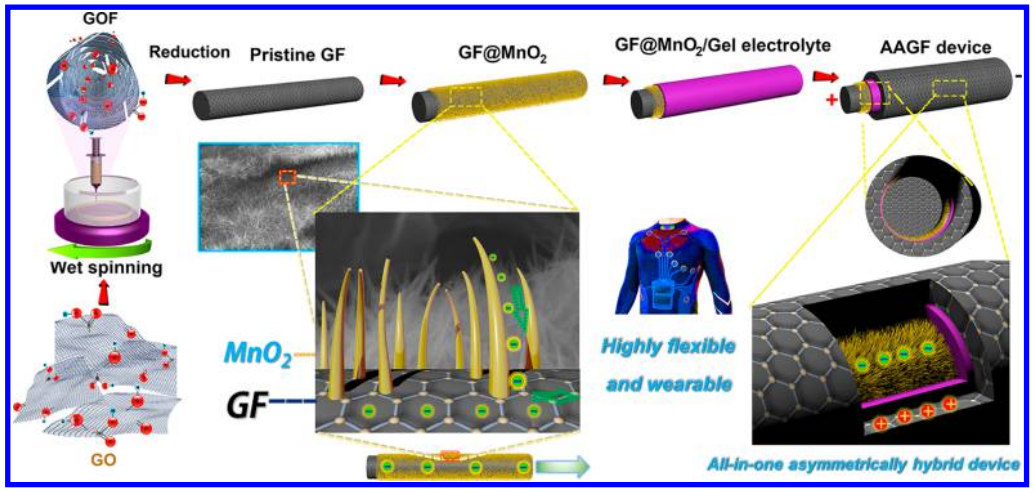

Figure 1. Schematic illustration of the fabrication route to AAGF device. Fabrication steps are wet spinning of graphene oxide fibers, reduction of fiber to form core GF, growth of MnO_2 layer, gel electrolyte coating, and outer graphene layer coating. SEM images of MnO_2 coating and structural schematics of AAGF are also shown.

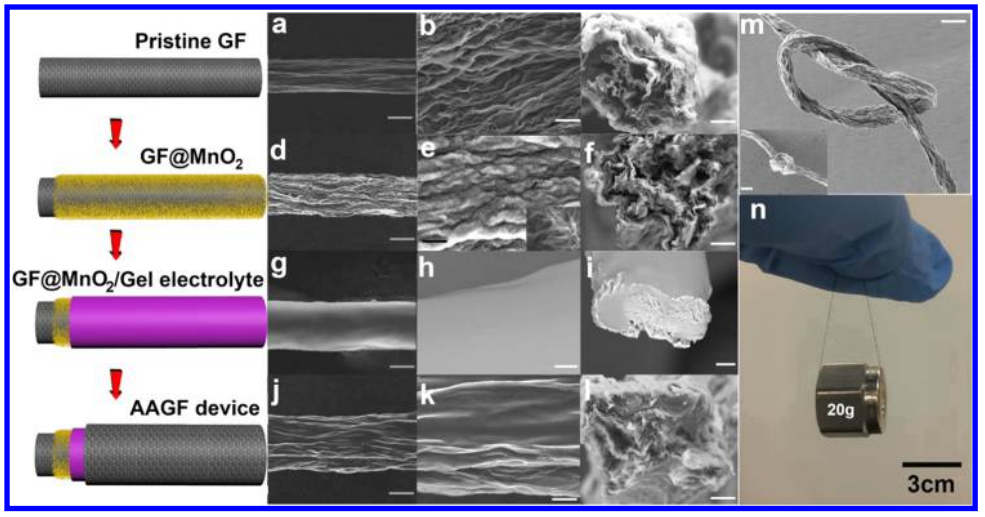

Figure 2. SEM of low (a, d, g, and j; scale bar 20 μm) and high (b, e, h, and k; scale bar 2 μm) magnification, cross-sectional image (c, f, i, and l; scale bar 10 μm) of pristine GF, GF@MnO_2, GF@MnO_2 with gel electrolyte, and AAGF device, respectively; the schematic illustrations correspond to the SEM image on their right side; (m) a loose and a tightened knot (inset image, scale bar 60 μm) of AAGF device; (n) real image of AAGF lifting a 20 g weight.

To solve these critical issues, herein we designed a novel all-in-one hybrid GF supercapacitor device. This device consists of a core GF electrode coated with hierarchically nanostructured MnO_2 layers, gel electrolyte of poly(vinyl alcohol) (PVA)/H_3PO_4, and sheath GF electrode, which are integrated into an all-in-one fiber device. This design, rather than intertwining two individual fibers, can effectively avoid circuit shortage and reduce the electron-transfer pathway. The electrolytic deposition of the MnO_2 thin film was conducted in neutral electrolyte solution in order to maintain the structural integrity of GF. The results showed that the introduction of hierarchical nanostructured MnO_2 dramatically increases the capacitance of GF device because of the occurrence of faradaic redox reaction in pseudocapacitance. The synergetic effect of graphene sheets and MnO_2 particles permits greater efficient electron transfer than that of double-layer capacitance on the basis of electrostatic adsorption/separation. Our triaxial all-in-one GF supercapacitor possesses not only a much higher specific volumetric capacitance of 29.6 F cm^{-3} without severe capacitance fading at high bending angle or high voltage scan rate but also remarkable flexibility and outstanding tensile strength that could be easily weaved into conductive textiles. The asymmetric GF supercapacitor also allowed for an extended operation voltage window of 1.8 V, resulting in a much higher energy density than that of other popular works based on all graphene fiber symmetric supercapacitor devices. This novel strategy also overcomes the high solution resistance of the conventional closely packed GO sheets. Therefore, the proposed novel all-in-one GF method holds great technological promise as an improved mean for constructing wearable supercapacitor devices.

RESULTS AND DISCUSSIONS

The details for the chemicals used, preparation of GO suspensions, process of wet-spinning, deposition of MnO_2 thin layers, fabrication of devices, instruments, and characterization approaches are given in the Supporting Information. To compare, all graphene symmetric GF (denoted SGF) all-in-one device, asymmetrically twisted GF (denoted TGF) device, and

DOI: 10.1021/acsami.7b10182
ACS Appl. Mater. Interfaces 2017, 9, 39576−39583

asymmetric GF (denoted AAGF) all-in-one device were prepared.

For energy-storage applications, it is believed that one-dimensional fiber materials can offer direct current pathways and shortened ion diffusion length, can enable large electrolyte−electrode contact area, can accommodate the volume expansion, and can impede mechanical degradation.[27,28] The synthetic routes to fabrication of all-in-one GF asymmetric supercapacitor are shown in the schematic of Figure 1. The core GF fiber was constructed via wet-spinning method (see details in Supporting Information) to be used as a structural support and current collector, followed by anodic deposition of hierarchically nanostructured MnO_2 on the as-prepared pristine GF. The middle layer of gel electrolyte and separator membrane was coated by dipping MnO_2 modified GF into PVA/H_3PO_4 viscous solution. The sheath GF was spontaneously formed by dipping as-prepared GF fiber into concentrated GO suspension and then by reducing it to rGO.

As scanning electron microscopy (SEM) shows in Figure 2a, compared to graphene oxide fiber (GOF) (Figure S1, Figure S2a), GF shrinks dramatically in radial direction after reduction by HI acid, showing a typically reduced diameter of 40 μm because of the loss of water or functional groups. The graphene sheets with characteristic wrinkles are uniform, closely and orderly packed along a consistent orientation. The high-magnification SEM of Figure 2b shows the homogeneously and uniformly distributed graphene sheets with a microporous, lamellar architecture. The cross-sectional SEM (Figure 2c) of GF reveals the unique closely packed and highly integrated structure, which further confirms the successful construction of a strong backbone GF. The macroporous structure and spacing between the graphene layers is beneficial for rapid adsorption/desorption of electrolyte ions in double-layer capacitance, which was evidenced by its excellent electrochemical performance discussed later.

Figure S2b shows a real photo of the neat GF (over 20 cm), the length of which is, in principle, only limited by the spinning time. Thus, mass production of pristine GF is commercially available via a constant extrusion approach. The as-prepared GF exhibited flexible characteristics, which allowed it to be deformed into circular, hexagonal, quadrilateral, or triangular shapes from a straight line (Figure S2d−g). Furthermore, the GF can be wrapped into coils and can be arranged in bundles (Figure S2c). The neat GF has high mechanical strength as the scaffold guarantees the flexibility of the generated AAGF fiber. Figure 2m shows AAGF tied in a loose knot, as it withstands the tension from the knot and remains intact. Interestingly, our neat GF can also be wrapped around a cylindrical stick or knotted along it without breaking (Figure S2h). The flexibility of the AAGF can allow it to be made into fabric and can serve as an excellent candidate for wearable electronics (Figure 1).

The mechanical strength of wet-spun GF is mainly determined by the amount of ion cross-linkage, covalent bonds, and van der Waals forces between adjacent rGO sheets. The utilization of large graphite precursors (over 200 um) permits much higher strength for GF versus a small size graphite. This can be attributed to more compact packing as well as to enhanced layer interaction between adjacent graphene sheets generated from large graphite, since larger graphite flakes allow for a larger contact surface area and stronger interlayer interactions. A strong GF is critical for stable, flexible, and highly conductive structures since less defects or fractures can facilitate electron transfer and thus can enhance performance. AAGF possesses even higher mechanical strength than GF because of the synergistic effects of PVA binding, and this was evidenced by lifting a 20 g of weight with AAGF without breaking (as in Figure 2n).

The coating of hierarchical MnO_2 was performed by the anodic deposition approach which is described in the Supporting Information. The anodic reactions in Mn-$(CH_3COO)_2$ electrolyte can be given as follows:[29]

$$Mn^{2+} + 2H_2O \rightarrow MnO_2 + 4H + +2e^- \quad (1)$$

As the SEM image shows in Figure 2d, the MnO_2 modified GF demonstrates a much rougher surface, compared with that of pristine backbone graphene fiber (Figure 2a). Hierarchical MnO_2 are homogeneously grown perpendicular to the GF surface, exhibiting a porous structure with numerous 2−5 μm pores evenly distributed throughout the entire fiber (Figure S3). This structure enhances the capacitive performance of GF@MnO_2 fiber by accommodating more active electrolyte ions as well as by shortening the electron-transfer pathway because of the unique one dimensional configuration. In addition, the existence of pores distributed throughout the GF material further confirms the lack of compact stacking between the graphene sheets. The higher magnification SEM image (Figure 2e) further reveals that the nanostructured, MnO_2 needles are homogeneously distributed on the surface of wrinkled graphene sheets substrate, which is also visually demonstrated in the 3D schematic of Figure 1. The ultrafine, nanostructured MnO_2 not only provides higher specific surface area to accommodate more ions involved in pseudocapacitance and double-layer capacitance during charge and discharge but also greatly increases the hydrophilicity of the GF surface to facilitate electrolyte diffusion and penetration, thus increasing the capacitive performance of the device.

PVA with H_3PO_4 was utilized as both electrolyte and membrane separator for the assembly of GF device. SEM images in Figure 2g show that PVA/H_3PO_4 is homogeneously assembled on GF@MnO_2 with an increased diameter of 90 μm. A higher magnification image (Figure 2h) reveals that the coated GF shows a smooth surface without defects, which is crucial for preventing short circuiting. For further observation, gel electrolyte coated GF@MnO_2 fiber was cut in liquid nitrogen for cross-sectional SEM characterization. Figure 2i demonstrates the arbitrary section of a broken gel electrolyte coated GF@MnO_2, confirming an even and smooth gel electrolyte coating. It can be clearly seen that the gel electrolyte partially penetrates into the outermost graphene layers and tightly enwraps the entire GF@MnO_2 without compromising the integrity of the structure, which facilitates ion diffusion and transfer between the positive and negative electrode. Moreover, the deep penetration of the gel electrolyte also enhances the mechanical strength of GF because of the high durability and superior tensile properties of PVA. The presence of this MnO_2 layer synergistically strengthens the gel coating because of its increased hydrophilicity compared to pristine graphene sheets. The homogeneous shrinking force of the PVA/H_3PO_4 sheath from the coaxial wet-spinning procedure enables the inner pore construction of GF@MnO_2 to be more elaborate.

The outer sheath coating of AAGF was achieved by dipping GF/MnO_2@PVA/H_3PO_4 into GO suspension followed immediately by a reduction process (Figure 1). The diameter of a typical AAGF is examined to be 120 μm as shown in Figure 2j. The SEM of AAGF (Figure 2j, k) demonstrates a less rough surface compared to pristine GF, which can be ascribed to the

DOI: 10.1021/acsami.7b10182
ACS Appl. Mater. Interfaces 2017, 9, 39576−39583

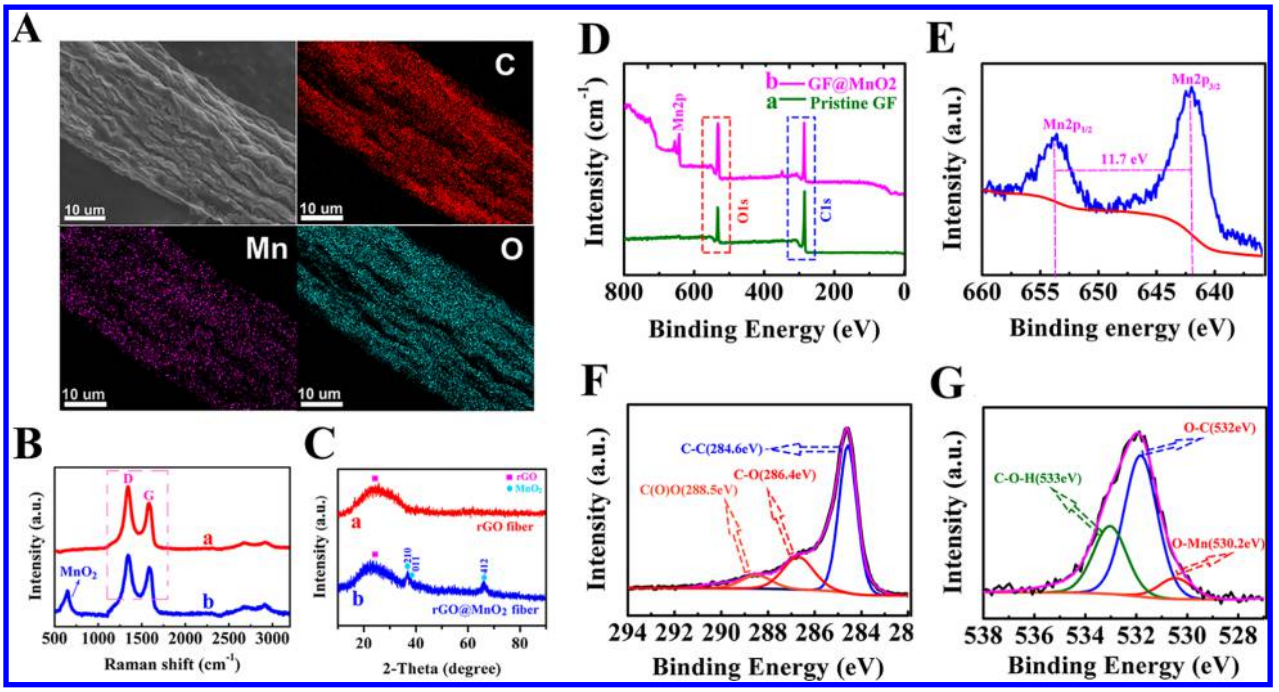

Figure 3. (A) Energy-dispersive spectroscopy (EDS) elemental mapping, (B) Raman spectroscope, and (C) X-ray diffraction pattern of (a) pristine GF and (b) GF@MnO_2. (D) XPS survey spectra of (a) the pristine GF and (b) GF@MnO_2; high-resolution XPS spectra for (E) Mn 2p, (F) C 1s, and (G) O 1s of the typical GF@MnO_2 sample.

penetration of PVA/H_3PO_4 into the out sheath graphene sheets. The close contact of gel electrolyte and outer sheath graphene sheets is beneficial for reducing charge-transfer resistance as well as for increasing mechanical strength of the entire device. This can be further proven by the cross-sectional image as shown in Figure 2l.

As SEM (Figure 3A) shows, observation of the hierarchical nanostructured MnO_2 thin layer on GF@MnO_2 presents difficulties because of the low deposited MnO_2 mass and small scale of the MnO_2 particles. Energy-dispersive spectroscopy (EDS) elemental mapping was employed in order to study the hybrid MnO_2/graphene composite. Figure 3 contains the original SEM image of GF@MnO_2, accompanied by the elemental mappings of C, Mn, and O (Figure 3A), which were obtained from the corresponding K-line energy densities in the same area. Homogenous and constant element dispersion covering the entire GF@MnO_2 backbone can be observed in elemental mapping of O and Mn, revealing the successful formation of MnO_2 thin film coating. Compared to Mn and O, C elemental map demonstrates higher distribution intensity, indicating the presence of a relatively thin layer of MnO_2 on the outward surface of GF. The relatively higher intensity of O element also indicates residual functional groups on GF after partial reduction of GOF. It has been proven that the existence of residual desirable oxygen atoms on rGO sheets can greatly benefit the capacitive performance of GF with enhanced wettability and additional pseudocapacitance.[30] Furthermore, uniformly distributed oxygen on the GF surface acts as hopping sites, facilitating the transfer of proton in slow kinetics faradaic reactions.[31] Also, high mass loading of MnO_2 coating is beneficial for enhancing pseudocapacitive capacitance but ultimately lowers the conductivity while making the GF more brittle (Figure S4). Thus, we compromise by growing a proper amount of hierarchical MnO_2 particles on GF to maintain the excellent mechanical properties while improving on capacitive performance. The cross-sectional image in Figure 2f shows that the thickness of MnO_2 attenuates along the radial direction of rGO fiber up to three to four graphene layers, which is ascribed to the decline of Mn^{2+} concentration with the increase in graphene layers. The number of coating layers or thickness is tunable by the adjustment of deposition time or electrolyte concentration.

Raman spectroscopy was employed for further confirmation of the presence of MnO_2 on GF. In Figure 3B, a, pristine GF shows the characteristic D band and G band at 1358 and 1511 cm^{-1}, respectively, which indicates a pure GF. For GF@MnO_2, as shown in Figure 3B, b, besides the characteristic D and G bands, the peaks at 572 and 634 cm^{-1} are ascribed to two different bond stretching modes, the (Mn−O) stretching vibration and the symmetric stretching vibration in the basal plane of the MnO_6 sheet,[32] which strongly suggests the existence of MnO_2 on the fiber. Furthermore, X-ray diffraction was carried out to examine the phase and structure of the GF before and after coating with MnO_2. Both pristine GF (Figure 3C, a) and GF@MnO_2 hybrid (Figure 3C, b) demonstrated a broad characteristic peak, which starts from 2θ = 16° to 2θ = 31°, where the center of the peak is located at 2θ = 24.5° with a *d*-spacing of 0.38 nm. The formation of this broad peak is attributed to shrinkage of the carbon frameworks on the GF sheets after the reduction process, resulting in a regain of van der Waals' interactions between the graphene sheets. The existence of this broad peak reveals that the reduced graphene sheets in GF are stacked in a highly disordered manner.[33] Apart from this, for the hybrid GF in Figure 3C, b, no obvious characteristic peaks from crystalline MnO_2 have been observed except for two broad and weak ones (2θ = 37.2° and 2θ = 67.3°), indicating that as-coated MnO_2 film contains both nanocrystalline and amorphous phases. The three diffraction peaks with weak intensity and broad characteristics are designated to (210), (011), and (412), which belong to

DOI: 10.1021/acsami.7b10182
ACS Appl. Mater. Interfaces 2017, 9, 39576−39583

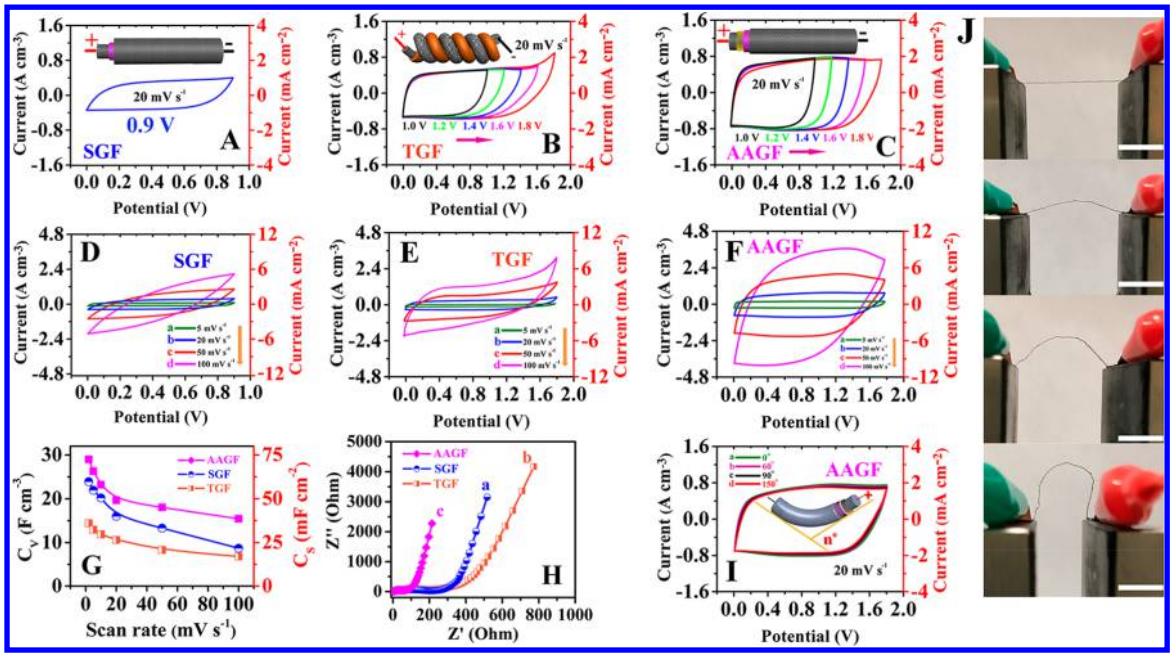

Figure 4. CVs of (A) SGF from 0 to 0.9 V, (B) TGF, and (C) AAGF from 0 to 1, 0−1.2, 0−1.4, 0−1.6, and 0−1.8 V at 20 mV s^{-1}; insets show the schematic of the devices; CVs of (D) SGF, (E) TGF, and (F) AAGF at different scan rates of 5, 20, 50, and 100 mV, respectively; (G) specific volumetric and areal capacitance and (H) impedance data of SGF, TGF, and AAGF, respectively; (I) bending test for AAGF from 0 to 150° at constant scan rate of 20 mV s^{-1}; (J) real photo of bend testing at different angles for AAGF (scale bar 2 cm).

orthorhombic MnO_2 crystal phase with a space group of *Pnma* (62) (JCPDS card no. 39-0375; *a*, 59.27 Å; *b*, 52.866 Å; and *c*, 54.533 Å).[34] Interestingly, no primary or strong peaks are observed in the as-coated MnO_2 diffraction pattern, revealing a reorientation of formed MnO_2 nanocrystallite. All the mentioned results sufficiently attest to a more amorphous nature of nanostructured MnO_2. It was found that amorphous MnO_2 powder electrodes exhibited ideal capacitive behavior and superior performance over the crystalline forms in aqueous solutions.[35,36] Thus, the presence of amorphous, hierarchical, and high surface area MnO_2 coatings should enhance the capacitive performance of GF.

Additionally, X-ray photoelectron spectroscopy (XPS) was performed in order to further study the chemical composition of GF@MnO_2. Compared to pristine GF, the hybrid GF@MnO_2 sample exhibits additional characteristic peaks from Mn 2p (Figure 3D) besides the C 1s and O 1s peaks from graphene. In Figure 3E, MnO_2 species from the GF@MnO_2 composite shows the high-resolution spectra, which clearly demonstrate that Mn 2p3/2 peak is indexed to 641.8 eV while Mn 2p1/2 peak is centered at 653.5 eV. The energy separation of the spin state between Mn 2p3/2 and Mn 2p1/2 is calculated to be 11.7 eV, which coincides with the published results of MnO_2,[37] confirming that Mn element exists as Mn(IV) valence state in GF@MnO_2 hybrid sample. In Figure 3F, three individual subpeaks constitute the characteristic peaks of high-resolution spectra of C 1s. These peaks indexed to 284.8, 286.2, and 288.5 eV can be attributed to carbon atoms belonging to graphitic sp2 hybridization and carbon atoms bonded to oxygen group. In Figure 3G, the main peak for O 1s splits into three subpeaks designated to O−Mn (530.2 eV), O−C (532.1 eV), and C−O−H (533.0 eV), which is in accordance with that of published results.[38] The confirmed residual oxygen functional groups introduce additional pseudocapacitance as well as maintain high wettability for the hybrid GF@MnO_2.

The electrochemical capacitive performance of GF devices was estimated by cyclic voltammetry (CV), electrochemical impedance spectroscopy (EIS), and galvanostatic charge−discharge (GCD) studies. To compare, SGF, TGF, and asymmetric AAGF devices (procedure in the Supporting Information) were prepared and investigated. SGF was constructed following the same procedure of AAGF only without coating hierarchical MnO_2, and TGF consisted of two intertwined individual 4 cm long GF@MnO_2 solidified in gel electrolyte (Figure S5), as the insets of Figure 4A and B show. CV of SGF from 0 to 0.9 V at constant scan rate of 20 mV s^{-1} in Figure 4A exhibits relatively low current, which corresponds to the unitary double-layer capacitance of pure graphene, and the voltage window of SGF is not extendable and limited to 1 V according to other literature. Figure 4B shows the CV curves of TGF device in variable operating voltage windows from 1 to 1.8 V at 20 mV s^{-1} scan rate, where the CV curves are rectangular and stable without obvious redox peak up to 1.4 V, indicating an ideal capacitive behavior. The operating voltage window of the asymmetric supercapacitor is able to be extended because of the introduction of overpotential of reversible hydrogen electrosorption in a nanoporous carbon-based negative electrode.[39] Polarization and distortion begin to appear from 1.6 to 1.8 V because of chemisorption of H^+ (OH^-) species on the negative (positive) electrode that modifies the work function difference.[40] CVs of AAGF in Figure 4C and F show a much larger area and more stable shapes without distortion from 1 to 1.8 V, compared with that of SGF Figure 4A, D and TGF Figure 4B, E. This indicates that our all-in-one assembly approach efficiently avoids the polarization of electrodes or evolution of hydrogen because of much larger contact area of electrodes and better penetration of electrolyte. Moreover, the introduction of MnO_2 nanostructures directly strengthens the capacitance of GF. In addition, rapid electrosorption of surface H^+ cations takes place in tandem with the quick and reversible faradic reaction between H^+ and

DOI: 10.1021/acsami.7b10182
ACS Appl. Mater. Interfaces 2017, 9, 39576−39583

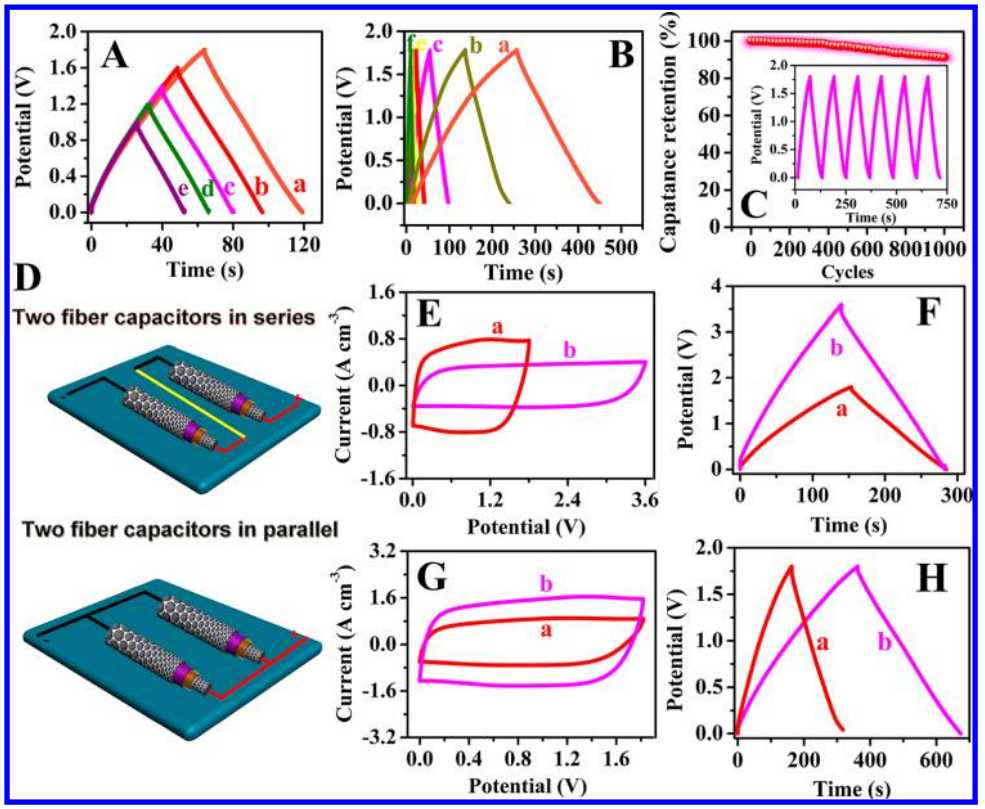

Figure 5. Galvanostatic charge/discharge curves of AAGF in (A) (a) 0−1 V, (b) 0−1.2 V, (c) 0−1.4 V, (d) 0−1.6 V, and (e) 0−1.8 V voltage windows at constant current density of 0.4 A cm^{-3} and (B) at (a) 0.1 A cm^{-3}, (b) 0.2 A cm^{-3}, (c) 0.4 A cm^{-3}, (d) 0.8 A cm^{-3}, (e) 0.9 A cm^{-3}, and (f) 1 A cm^{-3} in voltage window of 1.8 V. (C) Multiple charge−discharge cycling of AAGF and capacitance retention. (D) Schematic illustration of two AAGF in series and parallel; (E) CVs at scan rate of 20 mV s^{-1} and (F) galvanostatic charge/discharge curves at 0.2 A cm^{-3} of (a) single AAGF and (b) two AAGF in series; (G) CVs and (H) galvanostatic charge/discharge curves of (a) single AAGF and (b) two AAGF in parallel.

MnO_2.[41] The distortion of the current becomes severe when higher voltage scan rate is applied as Figure 4D, E shows. This can be ascribed to inefficient electrolyte ion diffusion or charge transfer under higher voltage scan rate. The specific volumetric specific capacitance calculated from CV data is shown in Figure 4G; 24.1, 14.9, and 29.6 F cm^{-3} for SGF, TGF, and AAGF were obtained at a scan rate of 2 mV s^{-1}, which declines to 8.9, 7.8, and 15.8 F cm^{-3} at a scan rate of 100 mV s^{-1}, respectively, further indicating that all-in-one assembly approach is beneficial for boosting the capacitive performance. Notably, this capacitance is comparable to or exceeds those of other peer works.[43−46] Moreover, the strong anchoring of MnO_2 nanoparticles on the graphene sheets facilitates rapid electron transfer between MnO_2 and the graphene substrate layer and enhances the electrochemical performance.[42]

Impedance data in Figure 4H testifies that the AAGF device surpasses the TGF device by much lower charge transfer resistance, which is attributed to the unique core−sheath electrode−electrolyte−electrode configuration. The flexibility of the prepared AAGF device was also examined by performing a bending test, which was carried out with a lab-made two-end bending machine equipped with a highly precise control system as shown in Figure 4J. The effect of bending on the electrocapacitive performance of the AAGF device was investigated by bending the AAGF device at variable angles. Interestingly, the CV curves at different angles were invariant and demonstrated insignificant change in a wide angle bent range from 0° (straight state) to 150° (Figure 4I), indicating that extensive and repetitive bending has a negligible impact on the capacitive performance. The excellent electromechanical stability of AAGF under bending suggests that this material has potential as a building block for flexible, large-area wearable devices. The CVs at scan rate of 20 mV s^{-1} are relatively constant, and little change occurs at different bending angles from 0° to 150°.

Real and imaginary capacitance calculated from EIS data further confirms the optimized design of our all-in-one device (Figure S6). Figure S6A illustrates that as frequency increases, the real part of the capacitance increase. Contrarily, an increase in frequency causes a maximum peak in the imaginary part of the capacitance (Figure S6B). The results reveal that the dispersion of the frequency dependencies is of relaxation type.[43] The optimized capacitance of MnO_2 coated AAGF device is evident in Figure S6A and S6B, which depicts that the device has an increase in capacitance while the scan rate is low and that the relaxation curve is shifted to higher frequencies.

Charge−discharge testing was carried out under chronopotentiometry at different current densities to examine full cell performance of our AAGF device (Figure 5A and B). The galvanostatic charge−discharge curves were analyzed at variable voltage windows from 1 to 1.8 V (Figure 5A) and at current densities (Figure 5B) from 0.1 to 1 A/cm^3 and by using multiple charge−discharge cycling (Figure 5C) in a voltage window of 1.8 V. The galvanostatic charge and discharge curves measured at either low or high current densities show relatively symmetric and straight lines, which reveal that our AAGF device possesses a perfect capacitance behavior. The linear charge−discharge behavior was achieved because of low impedance of the AAGF device, prepared for the first time using our novel all-in-one assembly method. Repeated cycling

DOI: 10.1021/acsami.7b10182
ACS Appl. Mater. Interfaces 2017, 9, 39576−39583

of AAGF shows excellent stability for 1000 cycles, maintaining 93% of initial capacitance. The low impedance is a result of the triaxial structure of AAGF device, in which the core strong GF provides strong structural support as well as high conductivity and the well-wrapped thin gel electrolyte reduces charge transfer and electrolyte resistance.

Our results reveal the outstanding performance of the AAGF flexible fiber supercapacitor device. To further stress the essentially pragmatic nature of our device, assembly of AAGF in series or in parallel has been prepared to evaluate the practical feasibility for integrating AAGF to wearable devices. As shown in Figure 5D, two AAGF wire supercapacitors are connected in series. The voltage window of the connected device is double that of the single wire AAGF, which is reflected on the CVs and charge−discharge curves (Figure 5E and F). The charge−discharge time of the integrating device is nearly constant compared to that of the single device. A parallel setup is also tested with two AAGF devices. As shown in Figure 5G and H, compared to the single AAGF device, as expected, the charge−discharge current density of the integrating device is enlarged two times. All these results testify to the feasibility of scaling up our fiber supercapacitors into a large piece of wearable device. Thus, our AAGF device can be potentially weaved into fabrics (Figure S7) without depreciating the performance of an individual wire device. Compared to TGF, the all-in-one configuration design of AAGF overcomes the inconvenience of large-scale assembly because of the uncovered gel electrolyte of TGF. Therefore, our new AAGF enables fabrication of high energy density storage devices with highly flexibility for wearing purpose.

CONCLUSIONS

In summary, an all-in-one GF based supercapacitor device with triaxial configuration has been successfully fabricated. The core backbone structure support GF exhibited extraordinary mechanical strength coupled with excellent conductivity. The coating of hierarchical nanostructured MnO_2 film not only introduced additional pseudocapacitance by providing abundant active sites exposed to the electrolyte but also increased the wettability for allowing penetration of sheath gel electrolyte PVA/H_3PO_4 into GF sheets. This design greatly benefits fast electron transfer during charge−discharge and enhancement of mechanical strength because of cross-linking from PVA. Our AAGF device exhibited stretchable and bendable mechanical properties with excellent electrocapacitive performance. A high volumetric capacitance of 29.6 F cm^{-3} can be observed at 2 mV s^{-1} scan rate, which is higher than most of the peer works. The capacitance of AAGF did not fade during bending testing from 0 to 150° with excellent capacitance retention of 93% after 1000 cycles. All of these characteristics make this design promising for wearable supercapacitors.

ASSOCIATED CONTENT

Supporting Information

The Supporting Information is available free of charge on the ACS Publications website at DOI: 10.1021/acsami.7b10182.

Experimental details and SEM images of pristine graphene fibers in various twisted and bent configurations as well as MnO_2 coated fibers and the frequency dependence of capacitance for all three devices (PDF)

AUTHOR INFORMATION

Corresponding Author

*E-mail: aipingyu@uwaterloo.ca.

ORCID

Zhongwei Chen: 0000-0003-3463-5509

Aiping Yu: 0000-0002-7422-7537

Author Contributions

‡L.L. and Y.L. contributed equally to this work.

Notes

The authors declare no competing financial interest.

ACKNOWLEDGMENTS

The authors greatly appreciate Prof. Zhongwei Chen and financial support from Natural Sciences and Engineering Research Council of Canada.

REFERENCES

(1) Sun, H.; You, X.; Deng, J.; Chen, X.; Yang, Z.; Ren, J.; Peng, H. Novel Graphene/Carbon Nanotube Composite Fibers for Efficient Wire-Shaped Miniature Energy Devices Adv. *Adv. Mater.* **2014**, *26* (18), 2868−2873.

(2) Lee, S.-Y.; Choi, K.-H.; Choi, W.-S.; Kwon, Y. H.; Jung, H.-R.; Shin, H.-C.; Kim, J. Y. Progress in Flexible Energy Storage and Conversion Systems, with a Focus on Cable-Type Lithium-Ion Batteries Energy Environ. *Energy Environ. Sci.* **2013**, *6* (8), 2414.

(3) Bognitzki, M.; Czado, W.; Frese, T.; Schaper, A.; Hellwig, M.; Steinhart, M.; Greiner, A.; Wendorff, J. H. Nanostructured Fibers Via Electrospinning Adv. *Adv. Mater.* **2001**, *13* (1), 70−72.

(4) Aleshin, A. N. Polymer Nanofibers And Nanotubes: Charge Transport And Device Applications Adv. *Adv. Mater.* **2006**, *18* (1), 17−27.

(5) Chabot, V.; Higgins, D.; Yu, A.; Xiao, X.; Chen, Z.; Zhang, J. A Review of Graphene and Graphene Oxide Sponge: Material Synthesis and Applications to Energy and the Environment Energy Environ. *Energy Environ. Sci.* **2014**, *7* (5), 1564.

(6) Liu, W.; Li, J.; Feng, K.; Sy, A.; Liu, Y.; Lim, L.; Lui, G.; Tjandra, R.; Rasenthiram, L.; Chiu, G.; Yu, A. Advanced Li-Ion Hybrid Supercapacitors Based on 3D Graphene−Foam Composites. *ACS Appl. Mater. Interfaces* **2016**, *8* (39), 25941−25953.

(7) Jun, Y.-S.; Sy, S.; Ahn, W.; Zarrin, H.; Rasen, L.; Tjandra, R.; Amoli, B. M.; Zhao, B.; Chiu, G.; Yu, A. *Carbon* **2015**, *95*, 653−658.

(8) Zheng, B.; Huang, T.; Kou, L.; Zhao, X.; Gopalsamy, K.; Gao, C. Graphene Fiber-Based Asymmetric Micro-Supercapacitors. *J. Mater. Chem. A* **2014**, *2*, 9736−9743.

(9) Cheng, H.; Hu, C.; Zhao, Y.; Qu, L. Graphene Fiber. *NPG Asia Mater.* **2014**, *6* (7), e113.

(10) Xu, Z.; Gao, C. Graphene Fiber: A New Trend in Carbon Fibers Mater. *Mater. Today* **2015**, *18* (9), 480−492.

(11) Zeng, W.; Shu, L.; Li, Q.; Chen, S.; Wang, F.; Tao, X. Fiber-Based Wearable Electronics: A Review of Materials, Fabrication, Devices, and Applications. *Adv. Mater.* **2014**, *26*, 5310−5336.

(12) Aboutalebi, S. H.; Jalili, R.; Esrafilzadeh, D.; Salari, M.; Gholamvand, Z.; Yamini, S. A.; Konstantinov, K.; Shepherd, R. L.; Chen, J.; Moulton, S. E.; Innis, P. C.; Minett, A. I.; Razal, J. M.; Wallace, G. G. High-Performance Multifunctional Graphene Yarns. *ACS Nano* **2014**, *8* (3), 2456−2466.

(13) Cheng, H.; Liu, J.; Zhao, Y.; Hu, C.; Zhang, Z.; Chen, N.; Jiang, L.; Qu, L. Graphene Fibers with Predetermined Deformation as Moisture-Triggered Actuators and Robots Angew. *Angew. Chem.* **2013**, *125* (40), 10676−10680.

(14) Lee, E. J.; Choi, S. Y.; Jeong, H.; Park, N. H.; Yim, W.; Kim, M. H.; Park, J.-K.; Son, S.; Bae, S.; Kim, S. J.; Lee, K.; Ahn, Y. H.; Ahn, K. J.; Hong, B. H.; Park, J.-Y.; Rotermund, F.; Yeom, D.-I. Active Control of All-Fibre Graphene Devices with Electrical Gating Nat. *Nat. Commun.* **2015**, *6*, 6851.

DOI: 10.1021/acsami.7b10182
ACS Appl. Mater. Interfaces 2017, 9, 39576−39583

(15) Meng, Y.; Zhao, Y.; Hu, C.; Cheng, H.; Hu, Y.; Zhang, Z.; Shi, G.; Qu, L. All-Graphene Core-Sheath Microfibers For All-Solid-State, Stretchable Fibriform Supercapacitors and Wearable Electronic Textiles. *Adv. Mater.* **2013**, *25*, 2326−2331.
(16) Bae, J.; Park, Y. J.; Lee, M.; Cha, S. N.; Choi, Y. J.; Lee, C. S.; Kim, J. M.; Wang, Z. L. *Adv. Mater.* **2011**, *23* (30), 3446−3449.
(17) Li, X.; Zang, X.; Li, Z.; Li, X.; Li, P.; Sun, P.; Lee, X.; Zhang, R.; Huang, Z.; Wang, K.; Wu, D.; Kang, F.; Zhu, H. Large-Area Flexible Core−Shell Graphene/Porous Carbon Woven Fabric Films For Fiber Supercapacitor Electrodes Adv. *Adv. Funct. Mater.* **2013**, DOI: 10.1002/adfm.201300464.
(18) Wang, X.; Liu, B.; Liu, R.; Wang, Q.; Hou, X.; Chen, D.; Wang, R.; Shen, G. Fiber-Based Flexible All-Solid-State Asymmetric Supercapacitors for Integrated Photodetecting System. *Angew. Chem.* **2014**, *126* (7), 1880−1884.
(19) Meng, F.; Lu, W.; Li, Q.; Byun, J.-H.; Oh, Y.; Chou, T.-W. Graphene-Based Fibers: A Review. *Adv. Mater.* **2015**, *27* (35), 5113−5131.
(20) Hu, Y.; Cheng, H.; Zhao, F.; Chen, N.; Jiang, L.; Feng, Z.; Qu, L. All-in-one graphene fiber supercapacitor. *Nanoscale* **2014**, *6* (12), 6448.
(21) Peng, Z.; Lin, J.; Ye, R.; Samuel, E. L. G.; Tour, J. M. Flexible and Stackable Laser-Induced Graphene Supercapacitors. *ACS Appl. Mater. Interfaces* **2015**, *7* (5), 3414−3419.
(22) Liu, Y.; Luo, D.; Ata, M. S.; Zhang, T.; Wallar, C. J.; Zhitomirsky, I. Universal dispersing agent for electrophoretic deposition of inorganic materials with improved adsorption, triggered by chelating monomers. *J. Colloid Interface Sci.* **2016**, *462*, 1−8.
(23) Peng, L.; Peng, X.; Liu, B.; Wu, C.; Xie, Y.; Yu, G. Ultrathin Two-Dimensional MnO2/Graphene Hybrid Nanostructures for High-Performance, Flexible Planar Supercapacitors. *Nano Lett.* **2013**, *13* (5), 2151−2157.
(24) Liu, Y.; Shi, K.; Zhitomirsky, I. Azopolymer triggered electrophoretic deposition of MnO2-carbon nanotube composites and polypyrrole coated carbon nanotubes for supercapacitors. *J. Mater. Chem. A* **2015**, *3* (32), 16486−16494.
(25) Liu, Y.; Zhitomirsky, I. Electrochemical supercapacitor based on multiferroic BiMn2O5. *J. Power Sources* **2015**, *284*, 377−382.
(26) Wu, Z.-S.; Ren, W.; Wang, D.-W.; Li, F.; Liu, B.; Cheng, H.-M. High-Energy MnO2Nanowire/Graphene and Graphene Asymmetric Electrochemical Capacitors. *ACS Nano* **2010**, *4* (10), 5835−5842.
(27) Mai, L.; Tian, X.; Xu, X.; Chang, L.; Xu, L. Nanowire Electrodes For Electrochemical Energy Storage Devices. *Chem. Rev.* **2014**, *114*, 11828−11862.
(28) Chan, C. K.; Peng, H.; Liu, G.; Mcilwrath, K.; Zhang, X. F.; Huggins, R. A.; Cui, Y. High-performance lithium battery anodes using silicon nanowires. *Nat. Nanotechnol.* **2008**, *3* (1), 31−35.
(29) Anothumakkool, B.; Kurungot, S. Electrochemically grown nanoporous MnO2 nanowalls on a porous carbon substrate with enhanced capacitance through faster ionic and electrical mobility. *Chem. Commun.* **2014**, *50* (54), 7188.
(30) Chen, Y.; Zhang, X.; Zhang, D.; Yu, P.; Ma, Y. High performance supercapacitors based on reduced graphene oxide in aqueous and ionic liquid electrolytes. *Carbon* **2011**, *49* (2), 573−580.
(31) Taberna, P. L.; Simon, P.; Fauvarque, J. F. Electrochemical Characteristics and Impedance Spectroscopy Studies of Carbon-Carbon Supercapacitors. *J. Electrochem. Soc.* **2003**, *150* (3), A292.
(32) Zhang, P.; He, M.; Xu, S.; Yan, X. The controlled growth of porous δ-MnO2nanosheets on carbon fibers as a bi-functional catalyst for rechargeable lithium−oxygen batteries. *J. Mater. Chem. A* **2015**, *3* (20), 10811−10818.
(33) Perera, S. D.; Mariano, R. G.; Nijem, N.; Chabal, Y.; Ferraris, J. P.; Balkus, K. J. Alkaline deoxygenated graphene oxide for supercapacitor applications: An effective green alternative for chemically reduced graphene. *J. Power Sources* **2012**, *215*, 1−10.
(34) Han, X.; Zhang, F.; Meng, Q.; Sun, J. Preparation and characterization of highly activated MnO2 nanostructure. *J. Am. Ceram. Soc.* **2010**, *93*, 1183−1186.
(35) Yu, A.; Chabot, V.; Zhang, J. *Electrochemical supercapacitors for energy storage and delivery: fundamentals and applications*; CRC Press: Boca Rotan, FL, 2013.
(36) Wei, W.; Cui, X.; Chen, W.; Ivey, D. G. Manganese Oxide-Based Materials as Electrochemical Supercapacitor Electrodes. *Chem. Soc. Rev.* **2011**, *40* (3), 1697.
(37) Zhu, S.; Zhang, H.; Chen, P.; Nie, L.-H.; Li, C.-H.; Li, S.-K. Self-assembled three-dimensional hierarchical graphene hybrid hydrogels with ultrathin β-MnO2 nanobelts for high performance supercapacitors. *J. Mater. Chem. A* **2015**, *3* (4), 1540−1548.
(38) Guo, D.; Dou, S.; Li, X.; Xu, J.; Wang, S.; Lai, L.; Liu, H. K.; Ma, J.; Dou, S. X. Hierarchical MnO2/rGO hybrid nanosheets as an efficient electrocatalyst for the oxygen reduction reaction. *Int. J. Hydrogen Energy* **2016**, *41* (10), 5260−5268.
(39) Ji, J.; Zhang, L. L.; Ji, H.; Li, Y.; Zhao, X.; Bai, X.; Fan, X.; Zhang, F.; Ruoff, R. S. Nanoporous Ni(OH)2Thin Film on 3D Ultrathin-Graphite Foam for Asymmetric Supercapacitor. *ACS Nano* **2013**, *7* (7), 6237−6243.
(40) Conway, B. E. *Electrochemical supercapacitors: scientific fundamentals and technological applications*; Springer Science & Business Media: New York, 2013.
(41) Yu, P.; Zhao, X.; Li, Y.; Zhang, Q. 3D Macroporous Nitrogen-doped Graphene Frameworks for High-Performance Supercapacitors. *MRS Online Proc. Libr.* **2014**, *1644*, 1644.
(42) Fan, Z.; Yan, J.; Wei, T.; Zhi, L.; Ning, G.; Li, T.; Wei, F. Asymmetric Supercapacitors Based on Graphene/MnO2 and Activated Carbon Nanofiber Electrodes with High Power and Energy Density. *Adv. Funct. Mater.* **2011**, *21* (12), 2366−2375.
(43) Xu, P.; Wei, B.; Cao, Z.; Zheng, J.; Gong, K.; Li, F.; Yu, J.; Li, Q.; Lu, W.; Byun, J.-H. Stretchable Wire-Shaped Asymmetric Supercapacitors Based on Pristine and MnO2Coated Carbon Nanotube Fibers. *ACS Nano* **2015**, *9* (6), 6088−6096.
(44) Zhang, Z.; Xiao, F.; Wang, S. Hierarchically structured MnO2/graphene/carbon fiber and porous graphene hydrogel wrapped copper wire for fiber-based flexible all-solid-state asymmetric supercapacitors. *J. Mater. Chem. A* **2015**, *3* (21), 11215−11223.
(45) Sun, G.; Zhang, X.; Lin, R.; Yang, J.; Zhang, H.; Chen, P. Hybrid Fibers Made of Molybdenum Disulfide, Reduced Graphene Oxide, and Multi-Walled Carbon Nanotubes for Solid-State, Flexible, Asymmetric Supercapacitors. *Angew. Chem.* **2015**, *127* (15), 4734−4739.
(46) Kötz, R.; Carlen, M. Principles and applications of electrochemical capacitors. *Electrochim. Acta* **2000**, *45* (15−16), 2483−2498.

DOI: 10.1021/acsami.7b10182
ACS Appl. Mater. Interfaces 2017, 9, 39576−39583